In vivo imaging of radial spoke proteins reveals independent assembly and turnover of the spoke head and stalk

Karl F. Lechtreck, Ilaria Mengoni, Batare Okivie, and Kiersten B. Hilderhoff

Department of Cellular Biology, University of Georgia, Athens 30602, GA

Author for correspondence: Karl F. Lechtreck Ph.D.
Cellular Biology
University of Georgia
635C Biological Science Building
120 Cedar Street, Athens, GA 30602
Phone 706-542 0167, FAX 706-542-4271
Email: lechtrek@uga.edu

Running title: Radial spoke transport

Keywords: axoneme, cilia, flagella, intraflagellar transport (IFT), RSP3, RSP4

Word count: 27,100 characters (without Material and Methods and References)

Abbreviations: IFT, intraflagellar transport; FP, fluorescent protein; mC, mCherry, mNG, mNeonGreen; mS, mScarlet-I; RS, radial spoke; RSP, radial spoke protein; sfGFP, superfolder GFP;

1

Abstract

1   Radial spokes (RSs) are multiprotein complexes regulating dynein activity. In the cell body and ciliary

2   matrix, RS proteins are present in a 12S precursor, which is converted into axonemal 20S spokes

3   consisting of a head and stalk. To study RS assembly *in vivo*, we expressed fluorescent protein (FP)-

4   tagged versions of the head protein RSP4 and the stalk protein RSP3 to rescue the corresponding

5   *Chlamydomonas* mutants *pf1,* lacking spoke heads, and *pf14,* lacking RSs entirely. RSP3 and RSP4

6   mostly co-migrated by intraflagellar transport (IFT). Transport was elevated during ciliary assembly.

7   IFT of RSP4-FP depended on RSP3. To study RS assembly independently of ciliogenesis, strains

8   expressing FP-tagged RS proteins were mated to untagged cells with, without, or with partial RSs.

9   RSP4-FP is added a tip-to-base fashion to preexisting *pf1* spoke stalks while de novo RS assembly

10   occurred lengthwise. In wild-type cilia, the exchange rate of head protein RSP4 exceeded that of the

11   stalk protein RSP3 suggesting increased turnover of spoke heads. The data indicate that RSP3 and

12   RSP4 while transported together separate inside cilia during RS repair and maintenance. The 12S RS

13   precursor encompassing both proteins could represent transport form of the RS ensuring stoichiometric

14   delivery by IFT. (196 of 200)

15

16   **Introduction**

17   The 9+2 axoneme is a highly ordered molecular machine conferring motility to cilia and flagella. While

18   providing stability to several μm-long flagella of just 200-nm in width, the axoneme is flexible to

19   execute complex waveforms with ~100 hz. Mutant analysis and proteomic studies have identified a

20   broad repertoire of axonemal proteins, which are synthesized in the cell body and transported into the

21   cilia (Lefebvre and Silflow, 1999; Pazour et al., 2005). How the cell body precursors of the axoneme

22   are transported and assembled remains largely unknown. Here, we study the assembly of radial spokes

23   (RSs), which project from the nine doublet microtubules toward the central pair and regulate the activity

24   of dynein by transmitting mechanical cues from the central pair (Oda et al., 2014). Mutations affecting

25   the RSs result in paralyzed flagella (pf) phenotypes in protists (Piperno et al., 1977; Vasudevan et al.,

26   2015) and cause primary ciliary dyskinesia in humans (Frommer et al., 2015). The RS consists of ~23

27   distinct proteins with diverse functional domain including several protein-protein interaction and

28   signaling protein motifs (Luck et al., 1977; Yang et al., 2006). During ciliary assembly, RS precursors

29   move from the cell body into the growing organelle. Intraflagellar transport (IFT), a bidirectional motor-

30   based motility of protein carriers has been implicated in RS transport but direct evidence is still missing

31   (Johnson and Rosenbaum, 1992; Qin et al., 2004).

32   Certain axonemal substructures move into cilia in form of multiprotein complexes. Inner and

33   outer dynein arms, for example, are preassembled in the cell body into complexes thought to contain all

34   subunits present in the corresponding mature structures inside cilia (Fowkes and Mitchell, 1998;

35   Viswanadha et al., 2014). Outer dyneins arms (ODAs) isolated from the cell body will dock at the right

36   sites onto the axoneme *in vitro* indicating that they are assembly competent and probably functional. In

37   contrast, RS assembly consists of two phases: First, a 12S complex is formed in the cell body and

38   transported into cilia (Qin et al., 2004). Inside cilia, the 12S complex is converted into the mature 20S

39   complex and docked onto the axonemal microtubules (Diener et al., 2011). During spoke maturation,

40 additional RS proteins that are not part of the 12S precursor (e.g., RSP16, HSP40 and LC8) are

41 incorporated (Gupta et al., 2012). However, how the Γ-shaped 12S particles is converted into the T-

42 shaped 20S RSs is unclear. The T-shaped RSs consist of the spoke head, the spoke neck, and the spoke

43 stalk with at least six, three, and nine subunits, respectively. A key structural protein of the stalk is

44 RSP3, whose N-terminus is close to microtubule-associated base of the spoke while the C-terminus

45 extends into the spoke head (Oda et al., 2014). Mutants lacking RSP3 assemble spoke-less axonemes.

46 The two wings of the spoke head are formed by homodimers of the paralogous proteins RSP4 and RSP6,

47 respectively. Mutants in RSP4 lack the spoke heads while the stalks are retained. Both head and stalk

48 proteins are part of the 12S RS precursor. How the 12S complex is converted into the mature 20s RS

49 remains unclear.

50   Here, we used fluorescent proteins (FP)-tagged RS proteins in *Chlamydomonas reinhardtii* to

51 analyze the transport and assembly of the RS. The head protein RSP4 and the stalk protein RSP3 are

52 transported by IFT and both proteins mostly co-migrate. However, both proteins are added with distinct

53 patters to the axoneme during RS assembly, turnover and repair. Our data indicate that RSP3 and RSP4

54 jointly enter the cilia, presumably in the previously characterized 12S complex, but separate inside the

55 cilium during RS repair and turnover. We propose that the 12S RS precursor presents a transport

56 complex of RS proteins.

57

58   **RESULTS**

59   *RSP4-sfGFP rescues the spoke-less pf1 mutant*

60   Using a derivate of the bicistronic vector pBR25, the spoke-head protein RSP4 was tagged at its C-

61   terminus with sfGFP and expressed in *C. reinhardtii pf1*, a mutant lacking endogenous RSP4 (Fig. 1A;

62   (Rasala et al., 2013)). As previously reported for RSP4-GFP, expression of RSP4-sfGFP rescued the

63   paralyzed flagella (*pf*)-phenotype in ~50% of the transformants analyzed (Fig. 1B; (Oda et al., 2014)).

64   TIRF imaging of live cells showed that RSP4-sfGFP was present along the entire length of the flagella

65   with exception of the very tip (Fig. 1C). For western blot analyses, we used an antibody raised against

66   RSP6, which also reacts with RSP4. RSP4 and RSP6 are paralogues sharing 47% identity and depend

67   on each other for assembly into flagella (Curry et al., 1992). In cilia of control cells, the antibody

68   recognized two bands corresponding to RSP4 and the somewhat smaller RSP6 (Fig. 1D). Both bands

69   were absent in the *pf1* mutant cilia. In the *pf1* RSP4-sfGFP rescue strain, the RSP6 band was retained

70   while the RSP4 band was replaced by two slower migrating bands. These bands also reacted with anti-

71   GFP and hence represent RSP4-sfGFP and uncleaved ble-RSP4-sfGFP; the amount of uncleaved ble-

72   RSP4-sfGFP varied between strains and preparations (Fig. 1b, d). In summary, expression of RSP4-

73   sfGFP restored wild-type motility in *pf1* suggesting that it can be used to monitor radial spoke (RS)

74   transport in living cells.

75

76   *RSP4-sfGFP is a cargo of IFT*

77   Previous data indicate that radial spokes move via IFT into cilia but the direct observation of this

78   transport has not yet been reported (Johnson and Rosenbaum, 1992; Qin et al., 2004). After

79   photobleaching of RSP4-sfGFP already incorporated into the flagella, IFT-like transport of RSP4-sfGFP

80   became visible (Fig. 2A). In steady-state flagella, anterograde IFT of RSP4-sfGFP was observed only

81   occasionally with a frequency of 0.6 transports/min. To study transport in growing flagella, cells were

82   deflagellated by a pH shock and allowed to initiate flagellar regeneration prior to mounting for TIRF

83   imaging. In such cells, the average anterograde transport frequency of RSP4-sfGFP was 10.4

84   transports/min and a maximum of 30 transports/min was observed (Fig. 2B, C). We conclude that

85   RSP4-sfGFP is a cargo of IFT and that RSP4 transport is strongly upregulated in regenerating flagella.

86

87   *RSP4 incorporates with distinct patterns into wild-type,* pf1, *and* pf14 *flagella*

88   In dikaryons obtained by mating *pf14* and wild-type gametes, the repair of RS-deficient *pf14* flagella

89   progresses from the tip toward the base as assessed using antibodies to RSP3 and RSP2 (Johnson and

90   Rosenbaum, 1992). The experiments suggest that radial spokes are transported by IFT to the flagellar

91   tip, where they are released followed by diffusion to axonemal docking sites. To study radial spoke

92   assembly *in vivo*, the *pf1* RSP4-sfGFP strain was mated to wild-type, *pf1*, and *pf14* gametes (Fig. 3A).

93   The zygotes possessed two GFP-positive flagella derived from the *pf1* RSP4-sfGFP donor strain and two

94   acceptor flagella initially devoid of GFP-tagged protein. In *pf1* RSP4-sfGFP x *pf1* zygotes, RSP4-sfGFP

95   was added in a pronounced tip-to-base pattern to the formerly *pf1* flagella (Fig. 3A a-b). Most cells

96   showed RSP4-sfGFP incorporation also in a small region near the flagellar base, a region for which IFT-

97   independent assembly of RSs has been proposed (Alford et al., 2013). Older zygotes are recognized by

98   the presence of shorter flagella, which progressively shorten during zygote maturation (Lechtreck et al.,

99   2013). In such zygotes, RSP4-sfGFP was equally or almost equally present along all four flagella

100   indicative for complete repair. The addition of RSP4-sfGFP to *pf14*-derived flagella of *pf1* RSP4-sfGFP

101   x *pf14* zygotes follows a distinct pattern: While often stronger near the tip, RSP4-sfGFP incorporation

102   was also present along the length of the *pf14*-derived flagella (Fig. 3A d-f). In matings with wild type,

103   RSP4-sfGFP was present in a spotted fashion along wild-type derived flagella (Fig. 3A g-j).

104   Kymograms revealed that these signals are stationary indicating stable docking of the protein to the

105   axoneme (Fig. 3B). More continuous signals representing RSP4-sfGFP were detected in the wild-type

106   derived cilia of older zygotes (Fig. 3A j). We conclude that untagged RSP4 was exchanged with RSP4-

107   sfGFP indicative of spoke head turnover. With ~2 events/min, the transport frequency of RSP4-sfGFP

108   in zygotic flagella was above that of non-regenerating flagella and below that of regenerating flagella.

109   Regardless of whether RSs were present, partially present (*pf1*), or absent (*pf14*), the transport

110   frequencies were similar indicating that RSP4-sfGFP transport is not regulated by the presence or

111   absence of intact RSs inside cilia (Fig. 3C).

112

113   *RSP4-sfGFP transport is highly processive*

114   The acceptor flagella of zygotes are well suited to image details of RSP4-sfGFP transport: They are

115   full-length allowing to study RS assembly independently of ciliogenesis and initially lack RSP4-sfGFP

116   incorporated in the axoneme making photobleaching unnecessary (Fig. 4A). Most RSP4-sfGFP

117   transport events progressed uninterrupted from the flagellar base to the tip (Fig. 4A, C). Anterograde

118   transport of RSP4-sfGFP progressed at typical IFT rates with an average velocity of 2.4 µm/s (STD 0.4

119   µm/s, n=256); retrograde transport was observed only rarely (Fig. 4A, B). Transitions from IFT to

120   diffusion and vice versa along the flagellar shaft were observed as well (Fig. 4A b). RSP4-sfGFP

121   arriving via IFT at the flagellar tip often remained stationary for extended times (Fig. S1). In detail,

122   RSP4-sfGFP remained in a distal position for ~1s (STD 0.4s, n=9) after arriving via IFT at the tip before

123   moving to a subdistal position, in which it remained for ~20 s or more (Fig. 4A; recordings typically

124   lasted for 30-60s). Such tip-bound particles were observed to regaining movement (Fig. 4A d)

125   suggesting RSP4-sfGFP often dwells for extended periods near the tip before moving into the flagellar

126   shaft. Apparent docking of RSP4-sfGFP onto *pf1* axonemes was rarely observed; the putative docking

127   events shown in Fig. 4A were preceded by extended periods of diffusion (Fig. 4A d). To summarize,

128   RSP4-sfGFP transport during the repair of *pf1* flagella is characterized by processive IFT to the tip,

129   prolonged dwelling at the tip, and extended diffusion prior to docking along the axoneme.

130

RSP3 is a cargo of IFT

Next, we rescued the *pf14* mutant by expression of RSP3 tagged at its N-terminus with mNeonGreen

(mNG); rescue was also observed for mScarlet-I (mS), mCherry (mC), and mTAG-BFP fusions (Fig.

5A). Similar to RSP4-sfGFP, mNG-RSP3 is transported by IFT; its transport frequency is elevated

during flagellar regeneration, and most transports progressed uninterrupted to the flagellar tip (Fig. 5B).

At the flagellar tip, mNG-RSP3 remained briefly stationary before the on-set of diffusion. In contrast to

RSP4-sfGFP, an extended stationary phase near the tip was not observed for mNG-RSP3 (Fig. 5B). In

matings with *pf14*, mNG-RSP3 was incorporated along the length of the *pf14*-derived flagella;

incorporation was somewhat stronger in the distal flagellar region (Fig. S2).

Biochemical studies in *C. reinhardtii* showed that RSP4 and RSP3 are both present in the 12S

RS precursor complex in the cell body (Diener et al., 2011; Qin et al., 2004). To analyze whether these

proteins remain associated during transport and assembly, we generated a strain expressing RSP3 and

RSP4 tagged with different FPs by mating *pf14* mC-RSP3 to *pf1* RSP4-sfGFP. The zygotes initially

possessed two red and two green flagella (Fig. 5C). At later time points, RSP4-sfGFP was readily

detected in the *pf14* mC-RSP3-derived flagella whereas only traces of mC-RSP3 were observed in the

pf1 RSP4-sfGFP derived flagella (Fig. 5C). The observation suggests that RSP3 and RSP4 in the wild-

type acceptor flagella are exchanged at distinct rates with the tagged proteins. A strain expressing both

RSP4-sfGFP mC-RSP3 in the corresponding double mutant background was identified among the

progeny of this cross by TIRF microscopy and western blotting (Fig. 5D).

150

During the repair of pf1 axonemes, RSP4 complexes are added to preexisting stalks

Flagella of *pf1* already possess RSP3-containing spoke stalks. The repair of *pf1* axonemes in dikaryons

could occur by the addition of spoke heads onto the preexisting stalks or by replacement of those stalks

154   with newly imported entire RSs; the outcome will potentially inform on the stability of the RSP3/RSP4-

155   containing RS precursor (Fig. 6A). To distinguish between these two possibilities, the mC-RSP3 RSP4-

156   sfGFP double strain was mated to *pf1* and wild-type gametes. In wild type-derived flagella of such

157   zygotes, both RS proteins were visible near the flagellar tip indicative for a limited turnover of the distal

158   axonemal segment as previously reported for tubulin (Fig. 6B a, b; (Harris et al., 2016; Marshall and

159   Rosenbaum, 2001). As described above, RSP4-sfGFP was also present in a spotted fashion along the

160   length of wild type-derived flagella indicative for the replacement of untagged RSP4 with the tagged

161   protein. In *pf1*-derived flagella, RSP4-sfGFP was readily visible in distal segments of early zygotes and

162   along most of the length in later zygotes indicative for tip-to-base assembly (Fig. 6B c-e). In contrast,

163   the signals representing mC-RSP3 in the mutant-derived flagella were generally weak including those of

164   late zygotes, which contained a near full complement of RSP4-sfGFP (Fig. 6B e). Apparently, RSP4-

165   sfGFP can be added to *pf1* flagella independently of mC-RSP3 incorporation. The data favor a model in

166   which RSP4-containing head complexes are added to the preexisting spoke stalks of *pf1* flagella (Fig.

167   6A.

168

169   *IFT of RSP4-sfGFP requires RSP3*

170   The observation that RSP4-sfGFP incorporates into *pf1* flagella without the apparent exchange of

171   untagged RSP3 with mC-RSP3 could be explained by the transport of a RSP4-sfGFP complex

172   independently of RSP3. First, we wanted to ensure that RSP3 and RSP4, which are both present in the

173   12S RS precursor complex, are indeed co-transported. RSP3 and RSP4 are thought to be dimers in the

174   mature spokes and probably the 12S precursor (Wirschell et al., 2008). While mNG and sfGFP tagged

175   version of RSP3 and RSP4 were readily detectable during transport, we were not able to detect mC-

176   RSP3transport, which could be explained by the low brightness and stability of mC. During the course

177   of this study, mScarlet I (mS), a novel bright monomeric red fluorescent protein, became available (Bindels et

178   al., 2017). Using mating, we generated a strain expressing mS-RSP3 and mNG-RSP4 in the

179   corresponding double mutant background (Fig. 7A). While still challenging, co-transport of tagged

180   RSP3 and RSP4 was observed in regenerating cilia (Fig. 7B, C). In 48 out of 60 analyzed IFT events,

181   mS-RSP3 co-migrated with RSP4-sfGFP including seven retrograde transports, six mS-RSP3 transports

182   lacked apparent RSP4-sfGFP, and for six mS-RSP3 transports it was unclear whether mNG-RSP4 was

183   associated or not. Co-migration of RSP3 and RSP4 was also observed in longer flagella, when only a

184   small share of the IFT trains carries RS proteins. The data support the notion that RSP3 is mostly in a

185   complex with RSP4 during IFT transport. However, we noted numerous mNG-RSP4 transports without

186   detectable co-migrating mS-RSP3 signal. The lack of mS-RSP3 signals is likely caused by technical

187   reasons, i.e., the comparatively low brightness and photostability of mS compared to mNG; also mNG

188   folds in <10 minutes while mS requires several hours to mature, which will prevent light emission from

189   mS-RSP3 newly translated during flagellar regeneration (Bindels et al., 2017; Shaner et al., 2013).

190   However, the observation could be also explained by RSP3-independent transport of RSP4.

191   Indeed, Diener et al. (2011) reported the presence of a RSP4/6/9/10 complex in the cell body cytoplasm

192   of *pf14* mutants indicating that near complete spoke heads assemble in the absence of RSP3. To test if

193   such head complexes travel via IFT, we expressed RSP4-sfGFP in *pf1 pf14* double mutants (Fig. 7D, E).

194   Anterograde and retrograde IFT of RSP4-sfGFP was sporadically observed in both steady state and

195   regenerating flagella but its frequency was exceedingly low (<0.01 events/minutes; Fig. 7D a). RSP4-

196   sfGFP occasionally remained stationary in *pf1 pf14* flagella indicative for association with the axoneme,

197   either unspecifically or by transient interaction with the central pair (Fig. 7D b). Finally, RSP4-sfGFP

198   often diffused inside the mutant flagella (Fig. 7D c, E). The data indicate that some RSP4-sfGFP can

199   enter the flagella independently of RSP3. However, the incorporation of RSP4-sfGFP into *pf1*-derived

200   mutant flagella occurs in a pronounced tip-to-base pattern presumably because the protein is shuttled via

201   IFT to the tip, where it will be released and diffuse to nearby docking sites. We think that neither low

202   frequency IFT nor entry of RSP4-sfGFP by diffusion is likely to explain that pattern observed during the

203   repair of *pf1* flagella; RSP4-sfGFP entering *pf1* flagella by diffusion should bind first to vacant sites near

204   the base of the cilium as described for *pf27*, a mutant lacking the putative RS-IFT adapter (Alford et al.,

205   2013).

206   Interestingly, RSP4-sfGFP accumulated near the basal bodies of many *pf1 pf14* RSP4-sfGFP

207   cells with steady state or regenerating flagella (Fig. 7E). In contrast to previous antibody-based studies,

208   an accumulation of RSP4-sfGFP and RSP3-sfGFP was not observed in the corresponding *pf1* and *pf14*-

209   derived rescue strains with growing or steady state flagella (not shown; (Qin et al., 2004)). Thus, the

210   build-up of RSP4-sfGFP at the basal bodies is likely to be related to the near complete failure to

211   associate to IFT in the absence of RSP3. In summary, in vivo imaging supports biochemical data that

212   the 12s RS precursor complex encompassing RSP3 and RSP4 is transported by IFT.

213

214   **Discussion**

215   Using direct *in vivo* imaging of FP-tagged RS proteins, we show that these proteins are transported by

216   IFT into *Chlamydomonas* flagella. The observations confirm previous studies indicating transport of RS

217   proteins to the flagellar tip by an active mechanism (Johnson and Rosenbaum, 1992). Also, RS proteins

218   have been shown to co-IP with IFT proteins from flagellar extracts (Qin et al., 2004). Direct

219   visualization of RS proteins during transport uncovered additional features of RS transport, which would

220   be difficult to determine by biochemical approaches. Both RS proteins tested here showed a high

221   propensity to move on IFT trains in one run from the flagellar base to the tip and the transport of both

222   proteins was upregulated during flagellar elongation. The data are reminiscent of previous observations

223   on the transport of FP-tagged tubulin and DRC4 and further support the notion that the amount of

224   axonemal proteins present on an IFT train is upregulated during flagellar growth (Craft et al., 2015;

225   Wren et al., 2013). The processivity of an IFT-cargo complex is likely to reflect the stability of the

226   interaction. Because different cargoes attach to distinct sites of the IFT particle, we expect differences

227   in the stability of the various IFT-cargo complexes (Bhogaraju et al., 2013; Lechtreck, 2015; Taschner et

228   al., 2017). Indeed, different cargoes showed distinct profiles in the distribution of unloading sites along

229   the flagellar length. Under the assumption that the distance traveled together reflects the stability of

230   IFT-cargo complexes, RSP4-IFT is more stable than DRC4-IFT and less stable than tubulin-IFT.

231   Two-color life imaging has shown transport of various proteins on IFT trains. The low-number

232   cargoes are typically tagged with bright and stable green-light emitting FPs whereas the IFT carriers

233   were tagged with red fluorescing proteins such as mCherry, which are not only less bright and

234   photostable but also more difficult to image due to the bright red autofluorescence of *C. reinhardtii*.

235   These shortcomings are mitigated by the fact that IFT trains are repetitive structures consisting of 15 -

236   40 IFT particles corresponding to a similar number of red FPs. Here, we accomplished simultaneous

237   imaging of RSP3 and RSP4, two low number cargo proteins. Even when transport of RSs occurred at a

238   low frequency as it is the case in longer regenerating flagella, most mS-RSP3 traveled in association

239   with mNG-RSP4 on the same IFT train. This suggests that both proteins are in a complex rather than

240   being associated independently of each other to different subunits of the IFT train. In comparison to

241   other axonemal proteins studied in our laboratory, both RS proteins were very difficult to image

242   presumably indicating a low number of active FPs in the transport unit.

243   Our *in vivo* imaging data are in agreement with previous biochemical data demonstrating a 12S

244   complex encompassing RSP3 and RSP4 in the cell body and flagellar matrix. Inside cilia, the 12S RS

245   precursor needs be transformed into the mature RSs; during this process, additional RS proteins are

246   recruited into the complex but most steps of the conversion mechanism remain unclear. It has been

247   suggested that two of the Γ-shaped 12S complexes will dimerize to form the scaffold of the largely

248   symmetric T-shaped RSs (Pigino and Ishikawa, 2012). Alternatively, the 12S precursor could be

249   remodeled into the 20S complex, e.g., by recruiting HSP40 and the dimeric 10-kDa protein LC8; LC8,

250   for example, could bind and stretch-out RSP3 dimers already present in the 12S precursor (Gupta et al.,

251   2012). The dimensions of the 12S complex (~28nm length and 20nm width) and of 20S spokes isolated

252   from axonemes (50nm length and 25nm width, each based on negative stain) support the notion that

253   more complex rearrangements are required to convert the 12S into the 20S complex (Diener et al.,

254   2011).

255   The current models of RS assembly assume that RSP3 and RSP4 present in a given 12S

256   precursor complex are not only transported together but also remain together during the conversion into

257   mature spokes. However, during the repair of the head-less stalks in *pf1*-derived flagella of dikaryons,

258   RSP4-sfGFP provided by the *pf1 pf14* RSP4-sfGFP mC-RSP3 donor strain incorporated without a

259   matching incorporation of mC-RSP3. This pattern suggests that RSP4-sfGFP separates at one point

260   from mC-RSP3 and is then added onto the existing untagged spoke stalks of the *pf1* axoneme. We also

261   observed that the incorporation of RSP4-sfGFP along the length of wild-type derived zygotic cilia

262   exceeded that of mC-RSP3. This indicates that untagged spoke heads were exchanged with newly

263   imported tagged ones while the untagged RS stalk remained in place.

264   One caveat of our approach is that the mC and mS tags are considerably weaker and less stable

265   than the sfGFP and mNG tags; thus, weaker FP-RSP3 signals could have been missed detection.

266   However, late zygotes possessed plenty of newly assembled RSP4-sfGFP along their entire length of the

267   *pf1*-derived acceptor flagella and both FP-proteins were prominently visible in the two donor flagella

268   and often near the tip of the acceptor flagella. Thus, the photochemical properties of the FPs are

269   unlikely to explain the near absence of mC-RSP3 signals in post-repair *pf1*-derived acceptor flagella.

270   The second caveat arises from the presence of untagged endogenous RSP3 in the zygotes. Cells could

271   favor untagged over tagged RSP3 during the assembly or transport of RS precursors. However, dual

272   tagged RSP3-RSP4 complexes were present and largely functional in the donor cell flagella. Further,

273   both RSP4-sfGFP and mC-RSP3 were observed near the tip of zygotic acceptor flagella demonstrating

274   transport and incorporation of mC-RSP3 even in the presence of endogenous RSP3 and our ability to

275   detect such signals.

276

277   It is unclear whether the proposed split of the 12S complex occurs only during the repair of head-less *pf1*

278   spokes and slow turnover of spoke heads in flagella with intact RSs or also during RS *de novo* assembly

279   in growing cilia and the repair of *pf14* flagella lacking spokes. During the repair of spoke-less *pf14*

280   flagella, tagged RSP3 and RSP4 appeared over the entire length of cilia with a somewhat stronger signal

281   near the tip. This observation is distinct from the tip-to-base repair pattern previously described for

282   RSP3 and RSP2 in *pf14* flagella based on antibody staining. We explain the differences with the

283   increased sensitivity of *in vivo* TIRF of unfixed cilia while immunofluorescence could accentuate the

284   somewhat higher density of RS proteins near the tip. In contrast, RSP4-FP is assembled in a

285   pronounced tip-to-base pattern onto *pf1* axonemes. However, both FP-tagged RS proteins mostly

286   dissociate from IFT at the ciliary tip from where they move into the ciliary shaft by diffusion. Thus, the

287   distinct pattern described above could indicate that the RSP4-containing head complexes are assembly-

288   competent once they leave the tip region and will diffuse and dock to the next available head-less stalk

289   they encounter. RSP3-complexes, however, need more time to mature and thus will diffuse deeper

290   down into the cilium before docking.

291   In summary, our data suggest that RSP3 and RSP4 enter cilia in a precomplex but separate into a

292   RSP3- and RSP4-containing subcomplexes before the formation of mature spokes. Co-transport of RS

293   proteins could ensure that they enter cilia in the proper stoichiometry. Also, IFT particles possess a

294   limited number of cargo binding sites favoring transport of complexes in which only one or a few of the

295   subunits directly interact with IFT. Within cilia, the separation of RSP3- and RSP4-subcomplexes could

296   aid in axonemal maintenance by facilitating the replacement of damaged or lost spoke heads. Current

297   data revealed similarities and differences in assembly, transport, and final mounting of axonemal dynein

298   and RSs; the future analysis of additional axonemal substructures promises to reveal additional

299   processes utilized to assemble axonemal substructures.

300

301   **Acknowledgements**

305

Materials and Methods

306

307 All strain were maintained in Minimal (M) medium (https://www.chlamycollection.org/methods/media-

308 recipes/minimal-or-m-medium-and-derivatives-sager-granick/) at 24 C with a light/dark cycle of 14/10

309 hours. The following strains were obtained from the Chlamydomonas Resource Center

310 (https://www.chlamycollection.org/): CC-613 (pf14 mt-), CC-1032 (pf14 mt+), CC-1024 (pf1 mt+),

311 CC-602 (pf1 mt-), CC-620 (nit1 nit mt+), and CC-621 (nit1 nit2 mt-).

312   For C-terminal tagging of RSP4 with super folder GFP (GFP), *RSP4* was amplified by PCR

313 using the primers RSP4f (CGCCTCGAGATGGCGGCAGTGGACAGC) and RSP4r

314 (CGCAGATCTGCTGCCGCCGCCGCTG) and the genomic RSP4-sfGFP construct described by ODA

315 et al. 2011 as a template. The cleaned PCR product was digested with Xho1 and BlgII, gel-purified, and

316 ligated into the pBR25-sfGFP-sfGFP vector (Lechtreck, 2016) digested with Xho1 and BamH1. This

317 placed the RSP4 CDS upstream of the gene encoding GFP. For N-terminal tagging of RSP4, the coding

318 sequence was amplified using the primers RSP4-f-Bgl2

319 (CGCAGATCTGGCGGCAGCGGCGGCATGGCGGCAGTGGACAGCG) and RSP4-r-EcoR1

320 (GCGGAATTCCTACTCGTCCGCCTCGGCCTC) and ligated downstream of the mNeonGreen (mNG)

321 gene using the pBR25-mNG-α-tubulin vector described in CRAFT et al. For N-terminal tagging of

322 RSP3, the *RSP3* coding region was amplified from a RSP3 cDNA clone using the primers RSP3f

323 (CGCGGATCCATGGTGCAGGCTAAGGCGCA) and RSP3r

324 (GCGGAATTCTTACGCGCCCTCCGCCTC). After digestion with BamH1 and EcoR1, the PCR

325 fragment was gel-purified and ligated into the pBR25-mNeon-α-tubulin vector digested with the same

326 enzymes (Craft et al., 2015). Derivates were obtained by replacing the mNeon gene with genes

327 encoding other FPs by restriction digest and ligation. Primers mScarlet-f-XhoI

328 (GCGCTCGAGATGGTGAGCAAGGGCGAG) and mScarlet-r-BamHI

329 (CGCGGATCCCTTGTACAGCTCGTCCATGCC) were used to amplify mScarlet-I (mS) using a

330   template codon-adopted for expression in mammalian cells. For transformation, the plasmids were

331   digested with Xba1 and Kpn1, the ble-RSP4-sfGFP and ble-mNeon-RSP3 cassettes were gel purified,

332   and introduced into appropriate strains (CC-602 and CC-1032) by electroporation. Transformants were

333   selected on zeocin plates (10 μg/ml), transferred to liquid medium, and analyzed for restoration of

334   motility. Expression of FP-tagged RS proteins was verified by TIRF microscopy and Western blotting.

335   A strain expressing both RSP4-sfGFP and mCherry (mC)-RSP3 was obtained by mating the

336   corresponding single rescue strains in CC-602 (RSP4-sfGFP *pf1* mt -) and CC-1032 (mC-RSP3 *pf14*

337   mt+). The progeny was screened by TRIF microcopy for expression of GFP and mC and Western

338   blotting was used to obtain *pf1 pf14* RSP4-sfGFP mC-RSP3 double mutant double rescue strain. The

339   *pf1 pf14* RSP4-sfGFP strain was isolated from the progeny of this cross. The *pf1 pf14* mNG-RSP4

340   mScarlet-RSP3 double mutant double rescue strain was generated following the same strategy.

341   For Western blot analyses, cells in HSM were deflagellated by the addition of dibucaine. After

342   removing the cell bodies by two differential centrifugations, flagella were sedimented 40,000 x g, 20

343   minutes, 4 C°. Flagella were dissolved in Laemmli SDS sample buffer, separated on Mini-Protean TGX

344   gradient gels (BioRad), and transferred electrophoretically to PVDF membrane. After blocking, the

345   membranes were incubated overnight in the primary antibodies; secondary antibodies were applied for

346   90-120 minutes at room temperature. After addition of the substrate (Femtoglow; Michigan

347   Diagnostics), chemiluminescent signals were documented using A BioRad Chemi Doc imaging system.

348   The following primary antibodies were used in this study: rabbit anti-RSP6 (Williams et al., 1986),

349   rabbit anti-RSP3 (Williams et al., 1989), rabbit anti-GFP (A-11122; ThermoFischer), mouse monoclonal

350   anti-IFT172 (Cole et al., 1998), and mouse monoclonal anti-IC2 (King and Witman, 1990).

351   Live imaging was performed on a Nikon eclipse Ti-U equipped with a 60x NA1.49 TIRF

352   objective, 488-nm and 561-nm diode lasers (Spectraphysics), a dual view system (Photometrics), and an

353   EMCCD camera (Andor iXon3). Data were collected using the Nikon Elements software package and

354   exported into Fiji for further analysis including kymography and frame extraction. Contrast and

355   brightness were adjusted in Fiji and in Photoshop and all figures were prepared in Illustrator (Adobe).

356   Specimen preparation, TIRF imaging, and data analysis have been described in detail in (Lechtreck,

357   2013) and (Lechtreck, 2016).

358   For flagellar regeneration experiments, 0.5 M acetic acid was rapidly added to cells in fresh M

359   medium under stirring (1,200 rpm) to reach a pH of ~4.25. After ~45s, KOH (0.25 M) was added to

360   neutralize the solution (pH ~6.8), the cells were collected by centrifugation, resuspended in M medium

361   and either used directly or stored on ice until needed. During regeneration, cells were incubated on a

362   shaker in bright light at room temperature. Specimens for live imaging were prepared 25 minutes after

363   the pH shock and later.

364   For mating experiments, cells were grown in bright light on M plates for ~9-12 days and then

365   transferred to dim light for 2-3days (see above for conditions). The evening before the experiment, cells

366   were resuspended in M-N medium (7-10 ml/plate) and incubated overnight in constant light with

367   agitation; agitation was omitted for the RS mutants, which assembled cilia better without shaking. In the

368   morning, cells were transferred to 1/5M-N supplemented with 10 mM Hepes pH 7 and incubated for an

369   additional ~2-6 hours. Gametes of opposite mating types were mixed in a microcentrifuge tube and

370   samples for imaging were taken over a period of ~5 minutes to several hours.

371

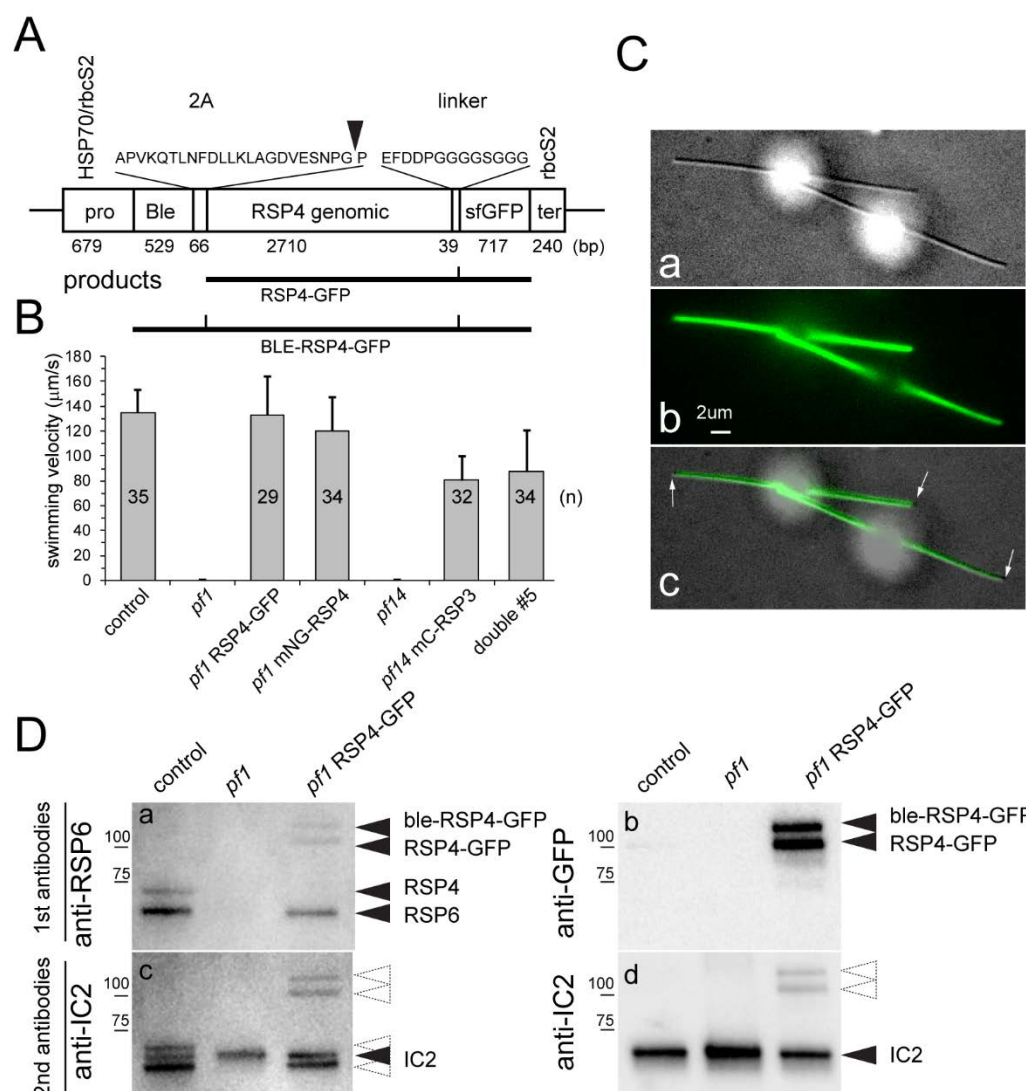372   **Figures with legends**

Figure 1

373

374   *Figure 1) RSP4-sfGFP rescues the pf14 mutant*

375   A) Schematic presentation of the bicistronic vector used to express RSP4-sfGFP. Due to incomplete

376   cleavage of the 2A sequence, the transformants expressed both RSP4-sfGFP and uncleaved ble-RSP4-

377   sfGFP.

378   B) Swimming velocity of wild type, and the *pf1* and *pf14* rescue strains. n, number of cells analyzed.

379   Note incomplete rescue of the motility phenotype in strains expressing mC-RSP3.

380   C) DIC (a), TIRF (b), and merged (c) image of a live cell expressing RSP4-sfGFP. Arrows indicate the

381   fkafellar tips lacking RSP4-sfGFP signal. Bar = 2μm.

382   D) Western blots analyzing flagella isolated from wild-type, *pf1*, and the *pf1* RSP4-sfGFP rescue strain.

383   The two replicate membranes (a/c and b/d) were first stained with anti-RSP6 (a) or anti-GFP (b) and

384   subsequently with anti-IC2, a component of outer arm dynein, as a loading control. The positions of

385   RSP6, RSP4, RSP4-sfGFP, ble-RSP4-sfGFP, and standard proteins are indicated. Dashed arrowheads

386   indicate residual signals from the first round of antibody staining.

387

Figure 2

388
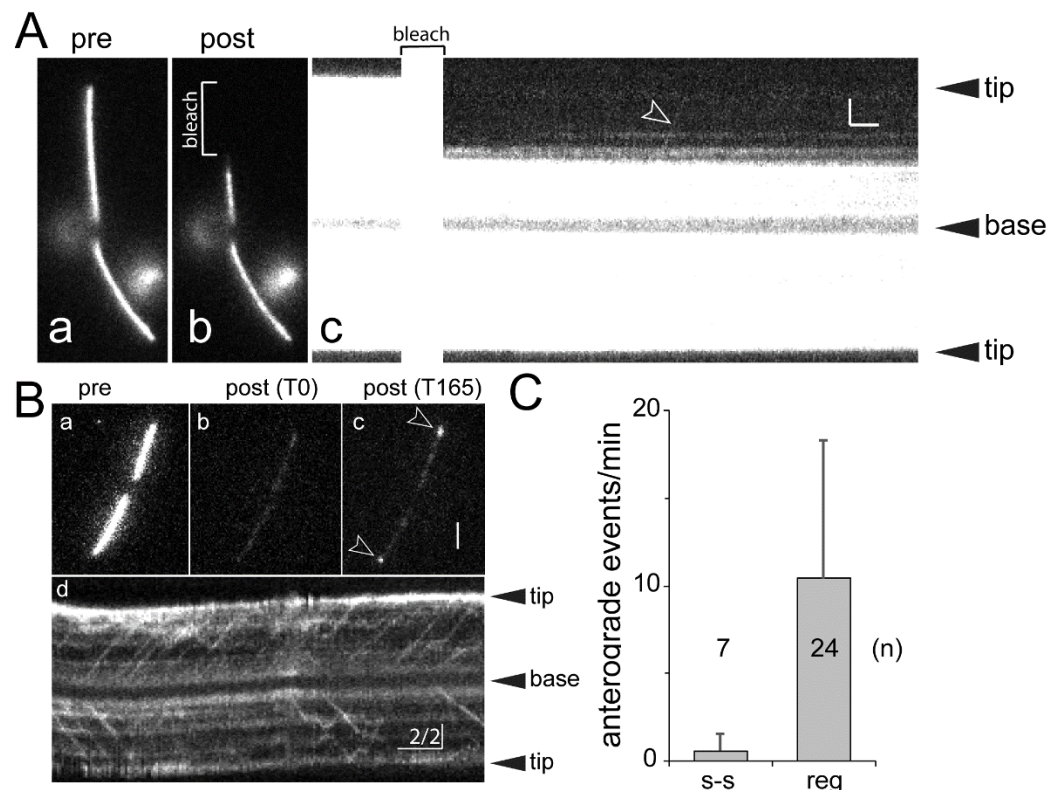
Figure 2) Transport of RSP4-sfGFP is upregulated during flagellar growth

A) Cell with steady-state flagella before (a) and after (b) photobleaching of the distal segment of one

flagellum (indicated by a bracket in b). The corresponding kymogram shows a single anterograde

transport event (arrowhead in c). Bars = 2s 2μm.

B) Cells during flagellar regeneration before (a), immediately after photobleaching (b, T0), and 165 s

after the bleach (c). Note incorporation of unbleached RSP4-sfGFP at the distal ends of both flagella

(arrowheads in c) indicative for axonemal elongation and spoke assembly. d) Kymogram of a

regenerating flagellum showing numerous transport events of RSP4-sfGFP. Bars = 2s 2μm.

C) Anterograde IFT events of RSP4-sfGFP observed in steady-state (s-s) and regenerating (reg) flagella.
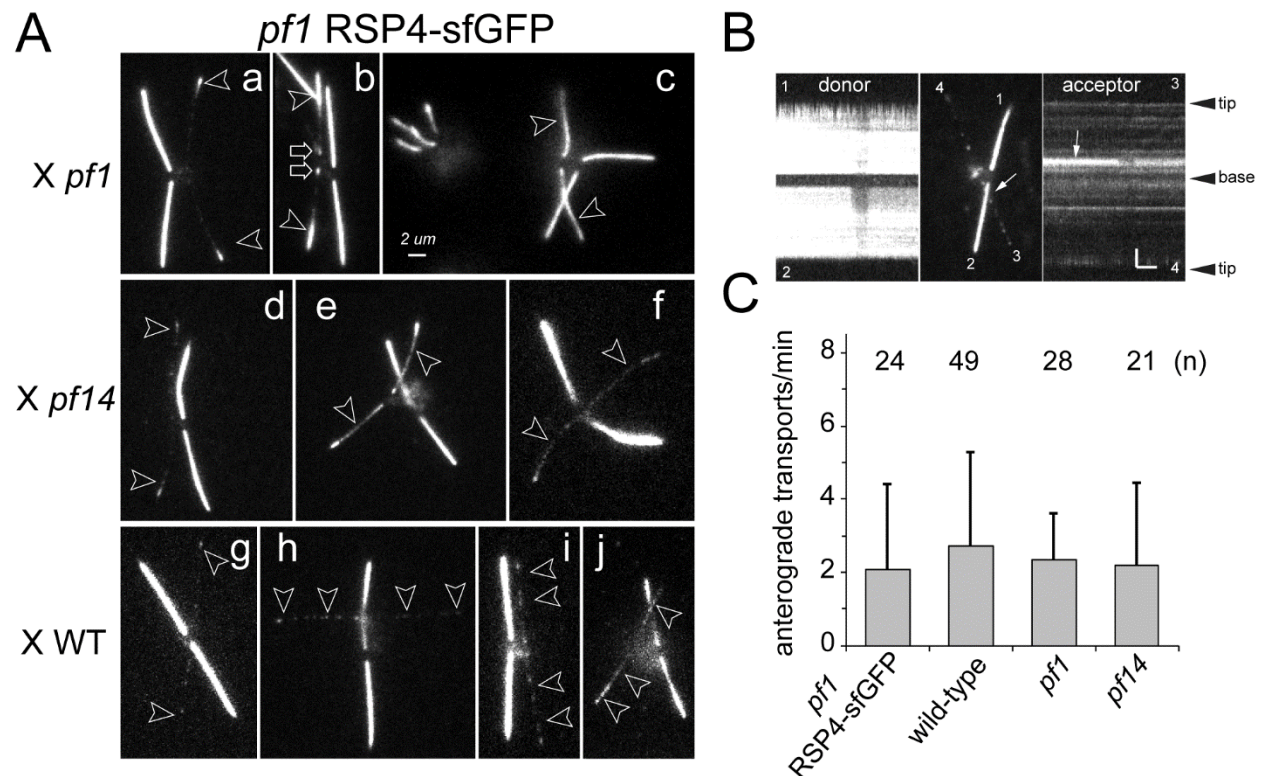
n, number of flagella analyzed.

399

Figure 3

Figure 3) RSP4-sfGFP incorporates with distinct patterns into pf1 and pf14 flagella

A) Gallery of still images of life zygotes from crosses between *pf1* RSP4-sfGFP and *pf1* (a-c), *pf14* (d-f), and wild type (WT, g-j). Acceptor flagella are marked by arrowheads. Late zygotes are shown in c; arrows in b mark proximal RSP4-sfGFP signals. Bar = 2μm.

B) Kymograms and still image of a *pf1* RSP4-sfGFP x wild type zygote. Horizontal trajectories in the acceptor flagella reveal that RSP4-sfGFP is stationary likely because of docking to the axoneme. Arrow: Crossing point of flagellum No. 2 and No. 3. Bar = 2 s 2 μm.

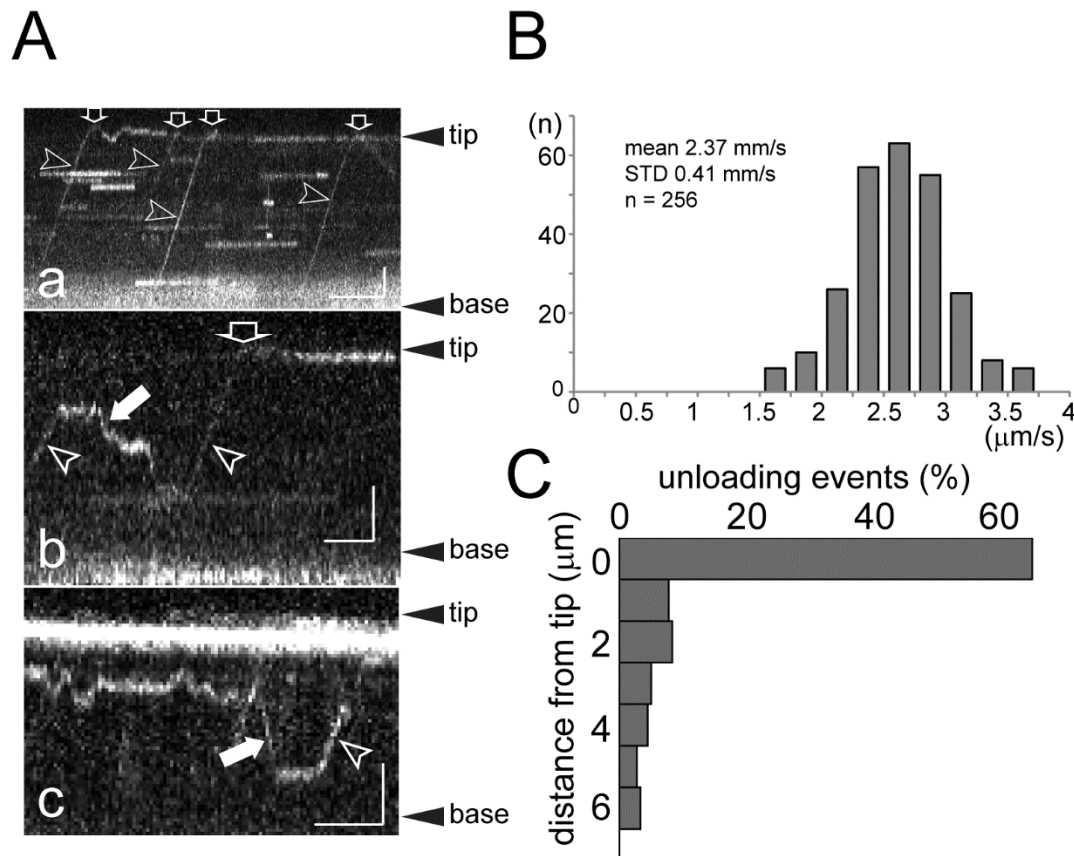C) Transport frequency of RSP4-sfGFP in zygotic flagella. n: number of flagella analyzed.

Figure 4

410

411   *Figure 4) RSP4-sfGFP is mostly transported to the flagellar tip.*

412   A) Gallery of kymograms depicting IFT transport to the flagellar tip (a), unloading and reloading (b),

413   dwelling at the tip (c), and retrograde transport. Arrowheads, anterograde transports; filled arrows,

414   retrograde transport; open arrows, arrival at the ciliary tip. Bars = 2s 2μm. See figure for additional

415   examples.

416   B) Distribution of the velocity of anterograde RSP4-sfGFP transports.

417   C) Distribution of IFT transport termination points of RSP4-sfGFP along the flagella. Note high share

418   of RSP4-sfGFP transport moving processively to the flagellar tip.

419

420

Figure 5

422
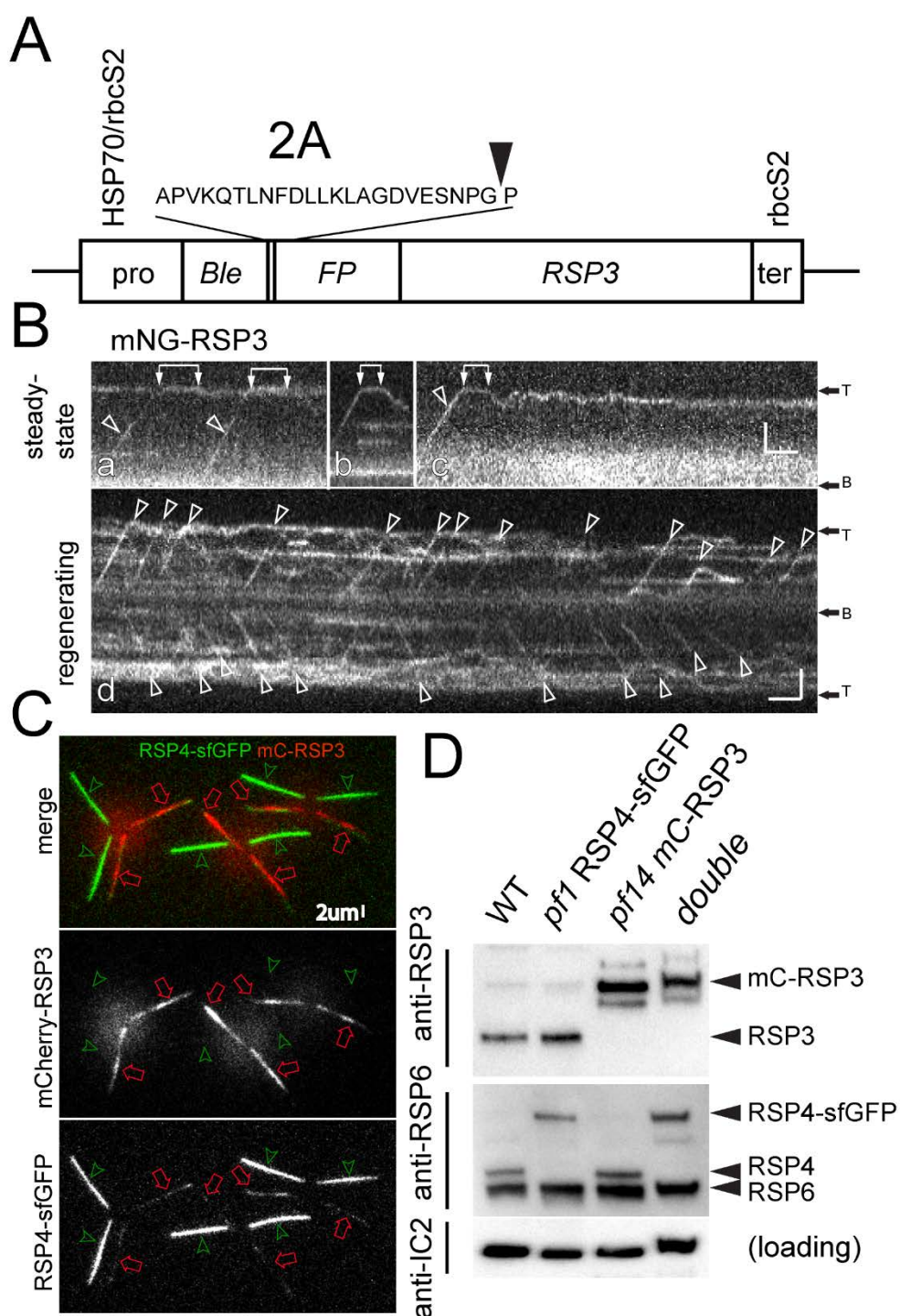
Figure 5) Generation of strain with two-color radial spokes

A) Schematic presentation of the vector used for FP-tagging of RSP3.

425   B) Kymograms showing mNG-RSP3 in steady-state (a-c) and regenerating (d) flagella. Transport

426   events are marked with arrowheads, interconnected pairs of white arrows indicate dwelling of mNG-

427   RSP3 at the flagellar tip. Bars = 2s 2μm.

428   C) Still image of three life *pf1* RSP4-sfGFP x *pf14* mC-RSP3zygotes. *pf1* RSP3-sfGFP and *pf14* mC-

429   RSP3 derived flagella are marked by green arrowheads and red arrows, respectively. Note incorporation

430   of RSP4-sfGFP along the length of the pf14 mC-RSP3 derived flagella. Bar = 2μm.

431   D) Western blots analyzing flagella isolated from wild-type (WT), *pf1* RSP4-sfGFP, *pf14* mC-RSP3,

432   and *pf1 pf14* RSP4-sfGFP mC-RSP3 (double) cells. Two replica membranes were stained with anti-

433   RSP3 and anti-RSP6 as indicated. Anti-IC2 staining was used to control for equal loading.
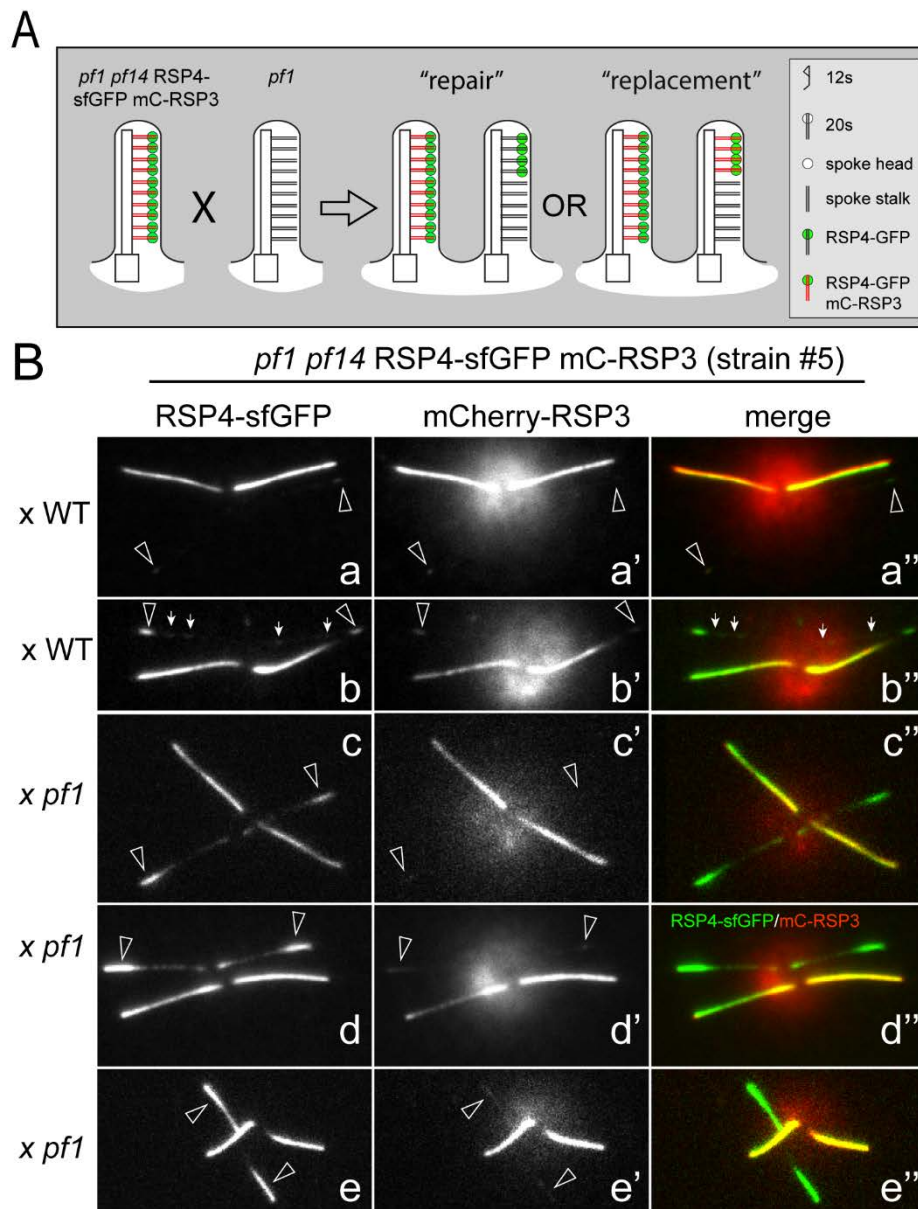
434

Figure 6

435

Fig. 6) RSP4 assembles into spoke head-deficient pf14 *flagella independently of RSP3*

A) Schematic presentation of the mating between the double strain (*pf1 pf14* RSP4-sfGFP mC-RSP3)

and *pf1*, and the possible outcomes, spoke repair by addition of RSP4-sfGFP heads or replacement with

newly imported entire mC-RSP3 RSP4-sfGFP spokes.

B) Gallery of images of zygotes obtained by mating the double mutant double rescue strain to either

wild-type (WT) or *pf1*. Shown are the sfGFP (a – e), mC (a' – e'), and merged (a'' – e'') images of life

442   cells. Arrowheads indicate the acceptor flagella. Small arrows, RSP4-sfGFP present in wild type-

443   derived flagella. The incorporation of mC-RSP3 is generally limited to the flagellar tip. Note near

444   absence of mC-RSP3 from the *pf14*-derived flagella of late zygotes, which possess RSP4-sfGFP along

445   their entire length (e). Bar = 2 μm.
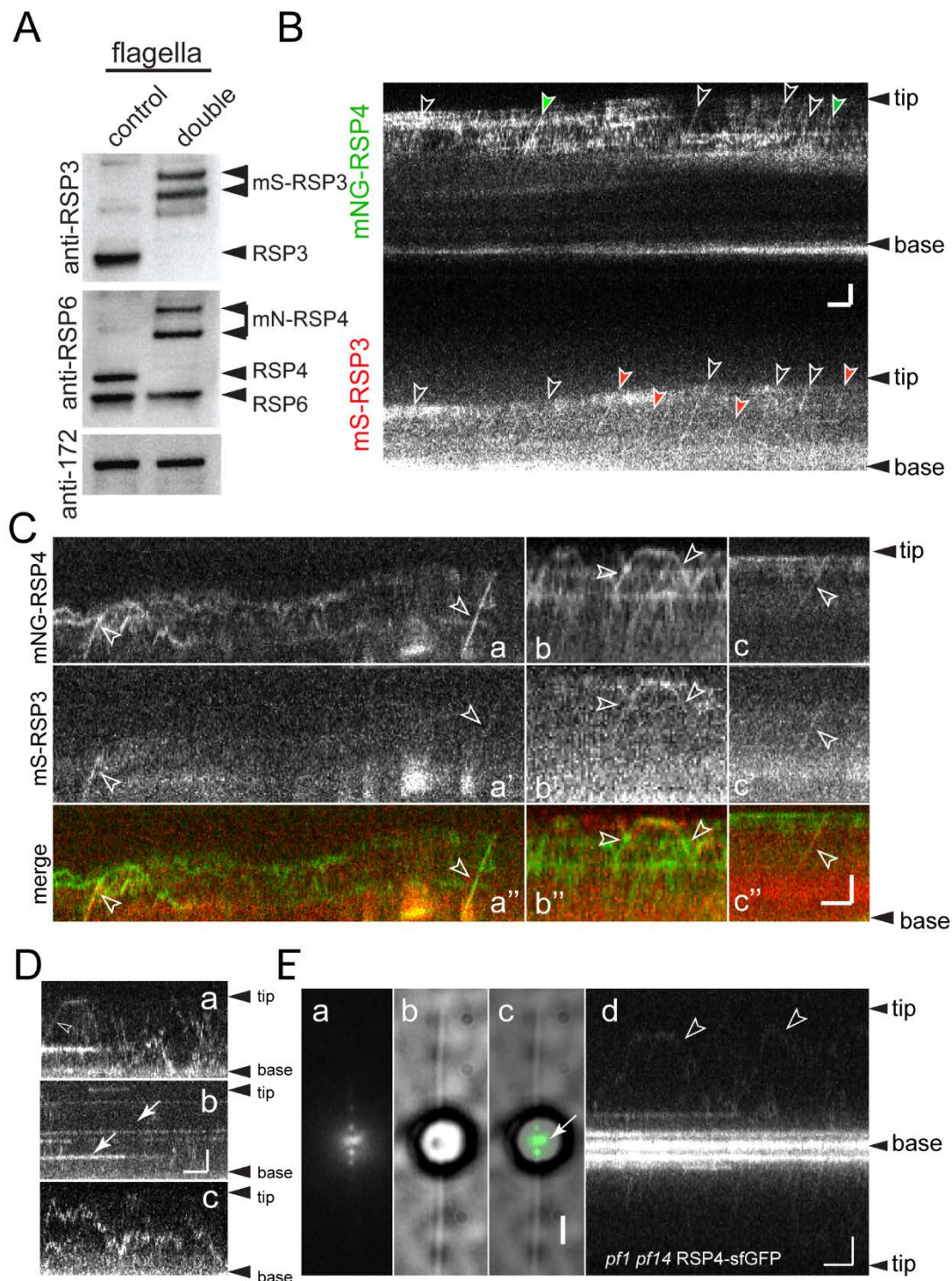
446

Figure 7

447

Figure 7) In the absence of RSP3, RSP4-sfGFP accumulates at the flagellar base

449   A) Western blots analyzing flagella isolated from a control strain of the *pf1 pf14* mS-RSP3 mNG-RSP4

450   double mutant double rescue strain. Two replica membranes were stained with anti-RSP3 and anti-RSP6

451   as indicated; anti-IC2 staining was used as a loading control.

452   B) Raw kymogram from a simultaneous recording of mS-RSP3 and mNG-RSP4 in regenerating flagella.

453   Co-transports are marked by open arrowheads. Colored arrowheads indicate transports visible only in

454   one of the two channels. Bar = 2s 2 μm.

455   C) Gallery of kymograms showing co-transport of mNG-RSP4 and mS-RSP3 in regenerating flagella.

456   Bar = 2s 2 μm.

457   D) Gallery of kymograms showing RSP4-sfGFP expressed in the *pf1 pf4* double mutant background in

458   regenerating (a, c – d) and steady-state (b) flagella. Arrowhead, Anterograde IFT. Arrows, Stationary

459   signals. Bar = 2s 2μm.

460   E) TIRF (10-frame image average), bright field, and merged image of a live *pf1 pf14* cell showing the

461   accumulation of RSP4-sfGFP near the basal bodies and in a spotted fashion in the proximal portions of

462   the flagella. Arrowheads RSP4-sfGFP diffusion. Bars = 2s 2μm.

463

464   **References**

465   Alford, L.M., A.L. Mattheyses, E.L. Hunter, H. Lin, S.K. Dutcher, and W.S. Sale. 2013. The Chlamydomonas mutant
466   pf27 reveals novel features of ciliary radial spoke assembly. *Cytoskeleton (Hoboken)*. 70:804-818.
467   Bhogaraju, S., L. Cajanek, C. Fort, T. Blisnick, K. Weber, M. Taschner, N. Mizuno, S. Lamla, P. Bastin, E.A. Nigg, and
468   E. Lorentzen. 2013. Molecular basis of tubulin transport within the cilium by IFT74 and IFT81. *Science*.
469   341:1009-1012.
470   Bindels, D.S., L. Haarbosch, L. van Weeren, M. Postma, K.E. Wiese, M. Mastop, S. Aumonier, G. Gotthard, A.
471   Royant, M.A. Hink, and T.W. Gadella, Jr. 2017. mScarlet: a bright monomeric red fluorescent protein for
472   cellular imaging. *Nat Methods*. 14:53-56.
473   Cole, D.G., D.R. Diener, A.L. Himelblau, P.L. Beech, J.C. Fuster, and J.L. Rosenbaum. 1998. Chlamydomonas
474   kinesin-II-dependent intraflagellar transport (IFT): IFT particles contain proteins required for ciliary
475   assembly in Caenorhabditis elegans sensory neurons. *J Cell Biol*. 141:993-1008.
476   Craft, J.M., J.A. Harris, S. Hyman, P. Kner, and K.F. Lechtreck. 2015. Tubulin transport by IFT is upregulated during
477   ciliary growth by a cilium-autonomous mechanism. *J Cell Biol*. 208:223-237.
478   Curry, A.M., B.D. Williams, and J.L. Rosenbaum. 1992. Sequence analysis reveals homology between two
479   proteins of the flagellar radial spoke. *Mol Cell Biol*. 12:3967-3977.
480   Diener, D.R., P. Yang, S. Geimer, D.G. Cole, W.S. Sale, and J.L. Rosenbaum. 2011. Sequential assembly of flagellar
481   radial spokes. *Cytoskeleton (Hoboken)*. 68:389-400.
482   Fowkes, M.E., and D.R. Mitchell. 1998. The role of preassembled cytoplasmic complexes in assembly of flagellar
483   dynein subunits. *Mol Biol Cell*. 9:2337-2347.
484   Frommer, A., R. Hjeij, N.T. Loges, C. Edelbusch, C. Jahnke, J. Raidt, C. Werner, J. Wallmeier, J. Grosse-Onnebrink,
485   H. Olbrich, S. Cindric, M. Jaspers, M. Boon, Y. Memari, R. Durbin, A. Kolb-Kokocinski, S. Sauer, J.K.
486   Marthin, K.G. Nielsen, I. Amirav, N. Elias, E. Kerem, D. Shoseyov, K. Haeffner, and H. Omran. 2015.
487   Immunofluorescence Analysis and Diagnosis of Primary Ciliary Dyskinesia with Radial Spoke Defects. *Am
488   J Respir Cell Mol Biol*. 53:563-573.
489   Gupta, A., D.R. Diener, P. Sivadas, J.L. Rosenbaum, and P. Yang. 2012. The versatile molecular complex
490   component LC8 promotes several distinct steps of flagellar assembly. *J Cell Biol*. 198:115-126.
491   Harris, J.A., Y. Liu, P. Yang, P. Kner, and K.F. Lechtreck. 2016. Single-particle imaging reveals intraflagellar
492   transport-independent transport and accumulation of EB1 in Chlamydomonas flagella. *Mol Biol Cell*.
493   27:295-307.
494   Johnson, K.A., and J.L. Rosenbaum. 1992. Polarity of flagellar assembly in Chlamydomonas. *J Cell Biol*. 119:1605-
495   1611.
496   King, S.M., and G.B. Witman. 1990. Localization of an intermediate chain of outer arm dynein by
497   immunoelectron microscopy. *J Biol Chem*. 265:19807-19811.
498   Lechtreck, K.F. 2013. In vivo imaging of IFT in Chlamydomonas flagella. *Methods Enzymol*. 524:265-284.
499   Lechtreck, K.F. 2015. IFT-Cargo Interactions and Protein Transport in Cilia. *Trends Biochem Sci*. 40:765-778.
500   Lechtreck, K.F. 2016. Methods for Studying Movement of Molecules Within Cilia. *Methods Mol Biol*. 1454:83-96.
501   Lechtreck, K.F., T.J. Gould, and G.B. Witman. 2013. Flagellar central pair assembly in Chlamydomonas reinhardtii.
502   *Cilia*. 2:15.
503   Lefebvre, P.A., and C.D. Silflow. 1999. Chlamydomonas: the cell and its genomes. *Genetics*. 151:9-14.
504   Luck, D., G. Piperno, Z. Ramanis, and B. Huang. 1977. Flagellar mutants of Chlamydomonas: studies of radial
505   spoke-defective strains by dikaryon and revertant analysis. *Proc Natl Acad Sci U S A*. 74:3456-3460.
506   Marshall, W.F., and J.L. Rosenbaum. 2001. Intraflagellar transport balances continuous turnover of outer
507   doublet microtubules: implications for flagellar length control. *J Cell Biol*. 155:405-414.
508   Oda, T., H. Yanagisawa, T. Yagi, and M. Kikkawa. 2014. Mechanosignaling between central apparatus and radial
509   spokes controls axonemal dynein activity. *J Cell Biol*. 204:807-819.
510   Pazour, G.J., N. Agrin, J. Leszyk, and G.B. Witman. 2005. Proteomic analysis of a eukaryotic cilium. *J Cell Biol*.
511   170:103-113.

512 Pigino, G., and T. Ishikawa. 2012. Axonemal radial spokes: 3D structure, function and assembly. *Bioarchitecture*.
513   2:50-58.
514 Piperno, G., B. Huang, and D.J. Luck. 1977. Two-dimensional analysis of flagellar proteins from wild-type and
515   paralyzed mutants of Chlamydomonas reinhardtii. *Proc Natl Acad Sci U S A*. 74:1600-1604.
516 Qin, H., D.R. Diener, S. Geimer, D.G. Cole, and J.L. Rosenbaum. 2004. Intraflagellar transport (IFT) cargo: IFT
517   transports flagellar precursors to the tip and turnover products to the cell body. *J Cell Biol*. 164:255-266.
518 Rasala, B.A., D.J. Barrera, J. Ng, T.M. Plucinak, J.N. Rosenberg, D.P. Weeks, G.A. Oyler, T.C. Peterson, F.
519   Haerizadeh, and S.P. Mayfield. 2013. Expanding the spectral palette of fluorescent proteins for the green
520   microalga Chlamydomonas reinhardtii. *Plant J*.
521 Shaner, N.C., G.G. Lambert, A. Chammas, Y. Ni, P.J. Cranfill, M.A. Baird, B.R. Sell, J.R. Allen, R.N. Day, M.
522   Israelsson, M.W. Davidson, and J. Wang. 2013. A bright monomeric green fluorescent protein derived
523   from Branchiostoma lanceolatum. *Nat Methods*. 10:407-409.
524 Taschner, M., A. Mourao, M. Awasthi, J. Basquin, and E. Lorentzen. 2017. Structural basis of outer dynein arm
525   intraflagellar transport by the transport adaptor protein ODA16 and the intraflagellar transport protein
526   IFT46. *J Biol Chem*. 292:7462-7473.
527 Vasudevan, K.K., K. Song, L.M. Alford, W.S. Sale, E.E. Dymek, E.F. Smith, T. Hennessey, E. Joachimiak, P.
528   Urbanska, D. Wloga, W. Dentler, D. Nicastro, and J. Gaertig. 2015. FAP206 is a microtubule-docking
529   adapter for ciliary radial spoke 2 and dynein c. *Mol Biol Cell*. 26:696-710.
530 Viswanadha, R., E.L. Hunter, R. Yamamoto, M. Wirschell, L.M. Alford, S.K. Dutcher, and W.S. Sale. 2014. The
531   ciliary inner dynein arm, I1 dynein, is assembled in the cytoplasm and transported by IFT before
532   axonemal docking. *Cytoskeleton (Hoboken)*. 71:573-586.
533 Williams, B.D., D.R. Mitchell, and J.L. Rosenbaum. 1986. Molecular cloning and expression of flagellar radial
534   spoke and dynein genes of Chlamydomonas. *J Cell Biol*. 103:1-11.
535 Williams, B.D., M.A. Velleca, A.M. Curry, and J.L. Rosenbaum. 1989. Molecular cloning and sequence analysis of
536   the Chlamydomonas gene coding for radial spoke protein 3: flagellar mutation pf-14 is an ochre allele. *J
537   Cell Biol*. 109:235-245.
538 Wirschell, M., F. Zhao, C. Yang, P. Yang, D. Diener, A. Gaillard, J.L. Rosenbaum, and W.S. Sale. 2008. Building a
539   radial spoke: flagellar radial spoke protein 3 (RSP3) is a dimer. *Cell Motil Cytoskeleton*. 65:238-248.
540 Wren, K.N., J.M. Craft, D. Tritschler, A. Schauer, D.K. Patel, E.F. Smith, M.E. Porter, P. Kner, and K.F. Lechtreck.
541   2013. A Differential Cargo-Loading Model of Ciliary Length Regulation by IFT. *Curr Biol*. 23:2463-2471.
542 Yang, P., D.R. Diener, C. Yang, T. Kohno, G.J. Pazour, J.M. Dienes, N.S. Agrin, S.M. King, W.S. Sale, R. Kamiya, J.L.
543   Rosenbaum, and G.B. Witman. 2006. Radial spoke proteins of Chlamydomonas flagella. *J Cell Sci*.
544   119:1165-1174.

545